Antti H. Niemi, Harri Hakula, and Juhani Pitkäranta. 2008. Point load on a shell. In: Karl Kunisch, Günther Of, and Olaf Steinbach (editors). Numerical Mathematics and Advanced Applications. Proceedings of the 7th European Conference on Numerical Mathematics and Advanced Applications (ENUMATH 2007). Graz, Austria. 10-14 September 2007. Springer, pages 819-826.

Point load on a shell

Antti H. Niemi, Harri Hakula and Juhani Pitkäranta

Abstract We study the fundamental (normal point load) solution for shallow shells. The solution is expressed as a Fourier series and its properties are analyzed both at the asymptotic limit of zero shell thickness and when the thickness has a small positive value. Some results of benchmark computations using both high- and low-order finite elements are also presented.

1 Introduction

According to the two-dimensional models of linear shell theory, the deformation of the middle surface of a thin shell under a given load is obtained by minimizing a quadratic energy functional of the form

$$\mathscr{F}(\mathbf{u}) = \mathscr{A}_m(\mathbf{u},\mathbf{u}) + \mathscr{A}_s(\mathbf{u},\mathbf{u}) + t^2\mathscr{A}_b(\mathbf{u},\mathbf{u}) - 2\mathscr{Q}(\mathbf{u}), \tag{1}$$

where t is the thickness of the shell and $\mathscr{A}_m$, $\mathscr{A}_s$, $t^2\mathscr{A}_b$ and $\mathscr{Q}$ correspond to the deformation energy due to stretching, deformation energy due to transverse shearing, deformation energy due to bending and the external load functional, respectively. Further, $\mathbf{u} = (u, v, w, \theta, \psi)$ is a vector field on the middle surface Γ of the shell that defines the tangential displacements u, v and normal deflection w of the middle surface as well as the rotations θ, ψ of its normal.

We consider here the problem of shell deformation under a normal point load so that the load functional is assumed to have the form

$$\mathscr{Q}(\mathbf{u}) = F\langle \delta_P, w\rangle = Fw(P), \tag{2}$$

Antti H. Niemi, Harri Hakula and Juhani Pitkäranta
Institute of Mathematics, Helsinki University of Technology, P.O.Box 1100, Espoo FI-02015 TKK, Finland, e-mail: antti.h.niemi@tkk.fi, harri.hakula@tkk.fi and juhani.pitkaranta@tkk.fi

where $P \in \Gamma$ is a point at the middle surface. The relevance of this problem is undeniable, as the solution is the fundamental solution, or *Green's function*, for normal loads and so it has been studied widely in classical shell theory, see e.g. [1] and the references therein. Anyway, it seems that closed form solutions have been obtained only for spherical shells and that the detailed behavior of the solution near point P is still an open problem when the thickness t is small — especially in hyperbolic and parabolic shell geometries.

Our aim here is to give some solutions to this problem and to find out how accurately these solutions can be approximated with finite elements. Our starting point is a 'shallow' version of the classical shell model where certain geometrical simplifications are assumed, see [6]. Within this simplified model, we analyze fundamental solutions that can be expressed as Fourier series and focus first on the asymptotic limit solution at $t = 0$. In model cases this can be expressed explicitly in the sense of distributions. We conclude that the transverse deflection w of the asymptotic solution has a term of the form $w \sim F\,\delta_P$ in all geometries. The remaining part of w is smooth when the shell is elliptic, but in hyperbolic and parabolic shell geometries there arises additional line δ-distributions along the characteristic lines of the middle surface.

Concerning the more realistic situation where the thickness t has a small positive value, we conclude as follows:

1. In all shell geometries the asymptotic term $w \sim F\,\delta_P$ is spread into a 'hot spot' of width $\sim \sqrt{Rt}$ around P, where R is the curvature length scale of the shell.
2. The line δ-distributions in the hyperbolic and parabolic cases are spread to 'ridges' of width $\sim \sqrt[n]{R^{n-1}t}$, where $n = 3$ in the hyperbolic case and $n = 4$ in the parabolic case.

We support these conclusions also by numerical experiments based on truncated Fourier series and finite element computations using both high- and low-order elements.

2 Classical shell theory

For a shell consisting of homogeneous isotropic material with Poisson ratio ν, the energy functionals in (1) are given by

$$\begin{aligned}
\mathscr{A}_m(\mathbf{u},\mathbf{u}) &= \int_\Gamma \left[\nu(\beta_{11}+\beta_{22})^2 + (1-\nu)(\beta_{11}^2+2\beta_{12}^2+\beta_{22}^2)\right] \mathrm{d}\Gamma, \\
\mathscr{A}_s(\mathbf{u},\mathbf{u}) &= \frac{1-\nu}{2}\int_\Gamma \left(\rho_1^2+\rho_2^2\right) \mathrm{d}\Gamma, \qquad (3) \\
\mathscr{A}_b(\mathbf{u},\mathbf{u}) &= \frac{1}{12}\int_\Gamma \left[\nu(\kappa_{11}+\kappa_{22})^2 + (1-\nu)(\kappa_{11}^2+2\kappa_{12}^2+\kappa_{22}^2)\right] \mathrm{d}\Gamma.
\end{aligned}$$

In a general geometry, the strains β_{ij}, ρ_i and κ_{ij}, $i,j=1,2$ are related linearly to the displacement components u,v,w,θ,ψ via variable coefficients that depend locally on the fundamental forms of Γ, see e.g. [1].

We assume here that the middle surface of the shell, in the neighborhood of point P, is represented in the form

$$z(x,y)=\frac{1}{2}ax^2+cxy+\frac{1}{2}by^2, \tag{4}$$

where x and y are Cartesian coordinates in the tangent plane Ω with origin P. The leading terms of the strain expressions at P may then be written as

$$\begin{aligned}
&\beta_{11}=\frac{\partial u}{\partial x}+aw, \quad \beta_{22}=\frac{\partial v}{\partial y}+bw, \quad \beta_{12}=\frac{1}{2}\left(\frac{\partial u}{\partial y}+\frac{\partial v}{\partial x}\right)+cw,\\
&\rho_1=\theta-\frac{\partial w}{\partial x}, \quad \rho_2=\psi-\frac{\partial w}{\partial y},\\
&\kappa_{11}=\frac{\partial \theta}{\partial x}, \quad \kappa_{22}=\frac{\partial \psi}{\partial y}, \quad \kappa_{12}=\frac{1}{2}\left(\frac{\partial \theta}{\partial y}+\frac{\partial \psi}{\partial x}\right).
\end{aligned} \tag{5}$$

The use of these expressions may be justified (formally, see [6]) also in a neighborhood of P, in which the middle surface Γ is shallow with respect to the tangent plane Ω, i.e. $r=\sqrt{x^2+y^2}$ is small compared with R. One may then as well set $\Gamma\hookrightarrow\Omega$ and $\mathrm{d}\Gamma\hookrightarrow \mathrm{d}x\mathrm{d}y$ when evaluating the strain energy functionals (3).

The above model can be simplified further by neglecting transverse shear energy which usually is small. This can be accomplished by eliminating the rotations θ,ψ from the classical *Kirchhoff-Love constraints*

$$\rho_1=\theta-\frac{\partial w}{\partial x}=0, \quad \rho_2=\psi-\frac{\partial w}{\partial y}=0. \tag{6}$$

The strain energy takes then the form

$$\mathscr{F}(\mathbf{u})=\mathscr{A}_m(\mathbf{u},\mathbf{u})+t^2\mathscr{A}_b(\mathbf{u},\mathbf{u})-2\mathscr{Q}(\mathbf{u}), \tag{7}$$

where now $\mathbf{u}=(u,v,w)$ and the bending strains are given by

$$\kappa_{11}=\frac{\partial^2 w}{\partial x^2}, \quad \kappa_{22}=\frac{\partial^2 w}{\partial y^2}, \quad \kappa_{12}=\frac{\partial^2 w}{\partial x\partial y}.$$

The minimizer of (7) satisfies the Euler equations

$$0 = -\frac{\partial \beta_{11}}{\partial x} - \nu \frac{\partial \beta_{22}}{\partial x} - (1-\nu)\frac{\partial \beta_{12}}{\partial y},$$

$$0 = -\nu \frac{\partial \beta_{11}}{\partial y} - \frac{\partial \beta_{22}}{\partial y} - (1-\nu)\frac{\partial \beta_{12}}{\partial x}, \tag{8}$$

$$F\delta_P = (a+\nu b)\beta_{11} + (\nu a + b)\beta_{22} + 2(1-\nu)c\beta_{12} + \frac{t^2}{12}\Delta^2 w,$$

where $\Delta = \frac{\partial^2}{\partial x^2} + \frac{\partial^2}{\partial y^2}$ is the usual two-dimensional Laplacian. These equations together constitute a system of total order eight and they can be expressed equivalently as the *fundamental shell equation*

$$\frac{t^2}{12}\Delta^4 w + (1-\nu^2)\Delta_m^2 w = F\Delta^2 \delta_P, \tag{9}$$

where Δ_m is a second order partial differential operator which represents membrane forces and is defined as

$$\Delta_m = a\frac{\partial^2}{\partial y^2} + b\frac{\partial^2}{\partial x^2} - 2c\frac{\partial^2}{\partial x \partial y}.$$

In view of (4) and the usual classification of differential operators, the operator Δ_m is called elliptic/hyperbolic/parabolic in accordance with the geometric nature of the middle surface at P. Note also that when $a = b = c = 0$, Eq. (9) reduces to the well known biharmonic equation representing the bending of a flat plate under a concentrated load.

To get an understanding of the curvature effects that couple membrane and bending action in shell deformations, we analyze solutions of (9) that can be expanded as Fourier series of the form

$$w(x,y) = \sum_{m,n=1}^{\infty} W_{mn} \cos\left((m-\tfrac{1}{2})\pi x\right) \cos\left((n-\tfrac{1}{2})\pi y\right). \tag{10}$$

Actually, this form was used already in [5], where we introduced a set of benchmark problems for the numerical evaluation of finite element algorithms.

Assume now that $P = (0,0)$ so that

$$F\delta_P(x,y) = F\sum_{m,n=1}^{\infty} \cos\left((m-\tfrac{1}{2})\pi x\right) \cos\left((n-\tfrac{1}{2})\pi y\right).$$

By using the shorthand notation $M = (m-\frac{1}{2})\pi$ and $N = (n-\frac{1}{2})\pi$, we may write formally $\Delta = -M^2 - N^2$ and $\Delta_m = -aN^2 - bM^2 - 2cMN$ in (9); hence, the Fourier coefficients of the transverse deflection are given by

$$W_{mn} = \frac{12F(M^2+N^2)^2}{t^2(M^2+N^2)^4 + 12(1-\nu^2)(aN^2+bM^2+2cMN)^2}. \tag{11}$$

We consider three model cases where the curvature parameters a,b,c are chosen as follows

1. $a=b=1/R$ & $c=0$ (Elliptic shell)
2. $c=1/R$ & $a=b=0$ (Hyperbolic shell, characteristic lines $x=0$ & $y=0$)
3. $b=1/R$ & $a=c=0$ (Parabolic shell, characteristic line $x=0$)

Let us study first the asymptotic limit solutions at $t=0$. In the classical shell-membrane theory one usually sets $t=0$ in (8) and then solves the system of equations by carefully relaxing the boundary and regularity conditions on $\mathbf{u}$. Here we do nicely by expanding the Fourier coefficients (11) at $t=0$ as follows:

1. $W_{mn}=\frac{FR^2}{1-\nu^2}$
2. $W_{mn}=\frac{FR^2}{1-\nu^2}\left(\frac{1}{2}+\frac{1}{4}\frac{M^2}{N^2}+\frac{1}{4}\frac{N^2}{M^2}\right)$
3. $W_{mn}=\frac{FR^2}{1-\nu^2}\left(1+2\frac{N^2}{M^2}+\frac{N^4}{M^4}\right)$

In $\Omega=(-1,1)\times(-1,1)$ these correspond to explicit solutions of the form

1. $w(x,y)=\frac{FR^2}{1-\nu^2}\delta_P(x,y)$
2. $w(x,y)=\frac{FR^2}{1-\nu^2}\left(\frac{1}{2}\delta_P(x,y)+\frac{1}{16}(|y|-1)\delta''(y)+\frac{1}{16}(|x|-1)\delta''(x)\right)$
3. $w(x,y)=\frac{FR^2}{1-\nu^2}\left(\delta_P(x,y)+\frac{1}{2}(|x|-1)\delta''(y)+\frac{1}{12}(|x|^3-3x^2+2)\delta''''(y)\right)$

Assume next that $t=\frac{1}{1000}$. We show in Figs. 1 and 2 contour plots of the deflection w in the hyperbolic and parabolic cases with the parameter values set as $R=1$, $\nu=\frac{1}{3}$ and $F=-1$. These results have been obtained by truncating the Fourier series (10), (11) at $m=n=1000$. We observe that in different shell geometries the main features of the deformations are rather similar close to P, but highly different away from P.

This behavior can be anticipated also from the Fourier coefficients (11). Namely, the curvature effects do not interact significantly with Fourier modes that vary in length scales $\ll\sqrt{Rt}\simeq 0.03$, but come into play when $M^2+N^2\sim\frac{1}{Rt}$ basically in the same way in any shell geometry. Concerning longer length scales, i.e. Fourier modes with $M,N<\frac{1}{\sqrt{Rt}}$, we may reason as follows. In the hyperbolic case one finds that

$$W_{mn}\sim\frac{12FM^2}{t^2M^6+48(1-\nu^2)R^{-4}},$$

when $N\sim R^{-1}$ so that W_{mn} grows with M until $M\sim\sqrt[3]{R^{-2}t^{-1}}$ and the same holds when the roles of M and N are exchanged. These properties are reflected in Fig. 1 as line layers decaying in the length scale $L\sim\sqrt[3]{R^2t}\simeq 0.10$ from the characteristic lines. In the parabolic case we have

$$W_{mn}\sim\frac{12FN^4}{t^2N^8+12(1-\nu^2)R^{-6}}$$

when $M\sim R^{-1}$ so that here W_{mn} grows with N until $N\sim\sqrt[4]{R^{-3}t^{-1}}$ in accordance with the line layer decaying in the length scale $L\sim\sqrt[4]{R^3t}\simeq 0.18$ in Fig. 2.

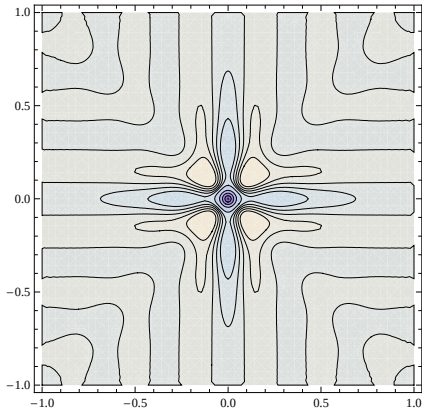

Fig. 1 Hyperbolic shell: Transverse deflection w at $t = \frac{1}{1000}$ due to the point load at $P = (0,0)$. Largest displacements take place within a 'hot spot' of width $\sim \sqrt{Rt} \simeq 0.03$ around P. In addition, the deformation features 'ridges' of width $\sim \sqrt[3]{R^2 t} \simeq 0.10$ along the characteristic lines $x = 0$ and $y = 0$.

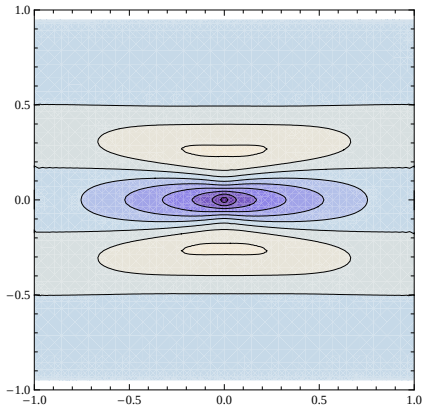

Fig. 2 Parabolic shell: Transverse deflection w at $t = \frac{1}{1000}$ due to the point load at $P = (0,0)$. Largest displacements take place within a 'hot spot' of width $\sim \sqrt{Rt} \simeq 0.03$ around P. In addition, the deformation features a 'ridge' of width $\sim \sqrt[4]{R^3 t} \simeq 0.18$ along the characteristic line $x = 0$.

3 Benchmark computations: *h*–FEM *versus* *p*–FEM

In this section, we construct finite element approximations to the fundamental solutions in the hyperbolic and parabolic cases. Since the imposition of the Kirchhoff-Love constraints (6) in a finite element space is rather complicated, we take the 5-field model (1)–(5) as our starting point here. We approximate each displacement component separately in the same way by using a standard scalar finite element space $V_{h,p} \subset H^1(\Omega)$ associated to subdivision of $\Omega = (-1,1) \times (-1,1)$ into rectangular elements with side length at most h and shape functions spanning all polynomials of given degree p, $p \geq 1$. On the boundary $\partial\Omega$, we impose as kinematic constraints the symmetry/antisymmetry conditions corresponding to (10), cf. [5].

We start by setting up two rectangular 'macroelement' meshes on Ω based on the specific structure of the solution in hyperbolic and parabolic cases, see Fig. 3. Our goal is to find out which is more efficient way to increase the accuracy of the approximation: raising the polynomial degree p within each macroelement or decreasing h in the lowest-order case ($p = 1$) by refining the mesh.

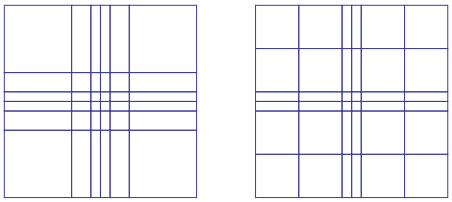

Fig. 3 Macroelement meshes for hyperbolic and parabolic shells at $t = \frac{1}{1000}$.

In the latter approach involving *bilinear* shape functions, we modify the transverse shear strains as

$$\rho_1 \hookrightarrow \Pi_x \rho_1, \quad \rho_2 \hookrightarrow \Pi_y \rho_2,$$

where Π_x and Π_y are defined elementwise as averaging operators in the coordinate direction indicated by the subscript so as to avoid *shear locking*. Among the possible numerical tricks aiming at avoiding *membrane locking*, we choose the one where the membrane strains are computed using the plane elastic strains on Ω:

$$\beta_{11} \hookrightarrow \Pi_x \beta_{11} + cR_y w, \quad \beta_{22} \hookrightarrow \Pi_y \beta_{22} + cR_x w,$$
$$\beta_{12} \hookrightarrow \frac{1}{2}\left(\tfrac{\partial u}{\partial y} + \tfrac{\partial v}{\partial x} + c\Pi_x w + c\Pi_y w + aR_x w + bR_y w\right).$$

Here R_x, R_y are certain difference operators, see [2, 3, 4] for more details on this formulation and its relation to current engineering practice.

We compare the above strategies by setting $p = 12$ in the 'p-version' and by subdividing each macroelement uniformly into 64 rectangles in the 'h-version' so that we have approximately 12000 degrees of freedom in both cases. The results of benchmark computations are reported in Figs. 4–6 showing the transverse deflection along the line $x = \frac{1}{2}$ as well as along the characteristic line $y = 0$ in hyperbolic and parabolic shell geometries. The results show that the 'h-version' is here clearly inferior to the 'p-version' — especially in resolving the line layer in hyperbolic geometry. In view of the theoretical predictions in [4], this is not so surprising.

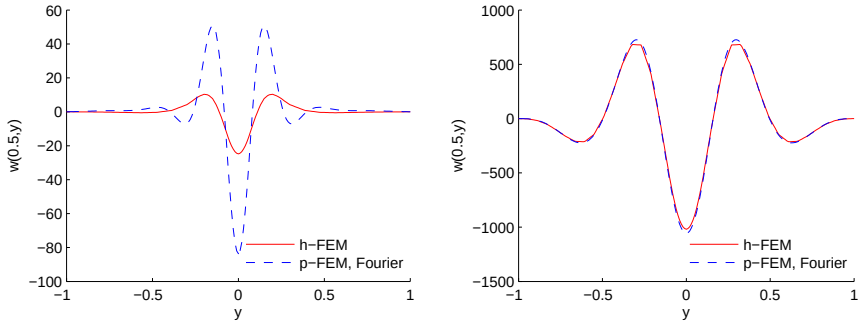

Fig. 4 Hyperbolic & Parabolic shells: Comparison of different methods along the line $x = \frac{1}{2}$.

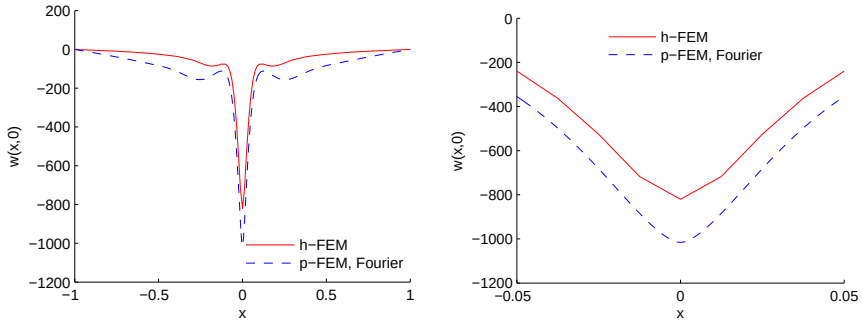

Fig. 5 Hyperbolic shell: Comparison of different methods along the characteristic line $y = 0$.

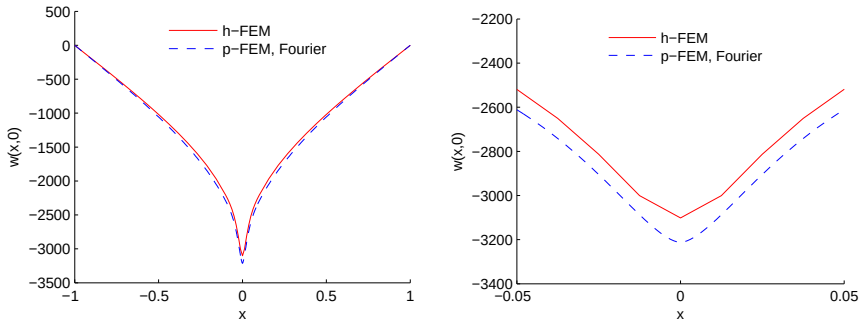

Fig. 6 Parabolic shell: Comparison of different methods along the characteristic line $y = 0$.

References

1. Lukasiewicz, S.: Local loads in plates and shells. Sijthoff & Noordhoff, The Netherlands (1979)
2. Malinen, M.: On the classical shell model underlying bilinear degenerated shell finite elements. Int. J. Numer. Meth. Engng **52**, 389–416 (2001)
3. Malinen, M.: On the classical shell model underlying bilinear degenerated shell finite elements: general shell geometry. Int. J. Numer. Meth. Engng **55**, 629–652 (2002)
4. Niemi, A.H.: Approximation of shell layers using bilinear elements on anisotropically refined rectangular meshes. Preprint submitted to Comput. Methods Appl. Mech. Engrg (2007)
5. Niemi, A.H., Pitkäranta, J., Hakula, H.: Benchmark computations on point-loaded shallow shells: Fourier vs. FEM. Comput. Methods Appl. Mech. Engrg. **196**, 894–907 (2007)
6. Pitkäranta, J., Matache, A.M., Schwab, C.: Fourier mode analysis of layers in shallow shell deformations. Comput. Methods Appl. Mech. Engrg. **190**, 2943–2975 (2001)